CURRENT DISTRIBUTION IN SUBMERGED ARC FURNACES FOR SILICON METAL / FERROSILICON PRODUCTION

G. Saevarsdottir[1] and J. A. Bakken[2]

[1] School of Science and Engineering, Reykjavik University, gudrunsa@ru.is.
[2] Department of Materials Science and Engineering, Norwegian University of Science and Technology

ABSTRACT

Current distribution in a Submerged Arc Furnace, is extremely important for the metallurgical processes, and overall furnace operation. This paper describes measurements of current and voltage on an industrial submerged arc furnace producing FeSi75. With a final goal of quantifying the fraction of furnace power generated in the electric arc, and furnace burden, a method was developed to quantify the fractional current in the electric arc and the current bypassing the arc through the charge respectively. The measurements treated in this paper were done on a 48 MVA industrial furnace at Elkem Icelandic Alloys plant in Iceland. Current and voltage waveforms were measured under normal operation, while the furnace was melted down and during start-up of the furnace on a coke bed. The measurements were compared to simulations employing an advanced MFD arc model. The time variability of the furnace resistance is used to estimate the current division between arc and charge. In particular electric arc resistance at current zero is evaluated, and used to estimate the charge resistance during metal production. The main results are that it is possible to use the time variability of phase resistance to distinguish between arc current and charge current. Using that the warmer chemically transformed part of an operating Si metal or FeSi furnace exhibits linear behaviour it is found that it passes close to 50% of the phase current, and similarly half of the furnace power is generated there.

1 INTRODUCTION

The metallurgical process in a SAF (Submerged Arc Furnace) producing Si or FeSi metal is extensively described by Schei et al. [1]. The process can be divided in two main steps. The metal producing, strongly endothermic step taking place in the crater zone, or the *inner reaction zone* of the furnace:

$$SiO_2 + aSiC = bSi + cSiO + dCO \tag{1}$$

requires temperatures around 2 000°C to run properly (equilibrium at 1 811°C). But before the charge materials reach the crater zone, they are chemically transformed at a lower temperature, the outer reaction zone, consuming carbon materials in order to produce silicon carbide SiC:

$$SiO + 2C = SiC + CO \tag{2}$$
$$2SiO = SiO_2 + Si \tag{3}$$

The reactions in the outer reaction zone are crucial, as all carbon raw materials should react to SiC before they reach the *inner reaction zone*, and capturing SiO gas before it reaches the surface of the hearth is critical for the Si recovery of the process. This transformation changes the properties of the hearth, the SiC being a good electrical conductor, and the condensed SiO_2 and Si metal coat the charge particles and promote electric current conduction through the charge. In addition, Iron sources in the raw materials for FeSi production influence the electrical behaviour of the charge considerably.

The current that passes through the electrodes into the SAF departs the electrode either through electric arcs or through direct contact between the charge and electrode. The electric power in the furnace is dissipated by Ohmic heating. The electric arc has a core temperature above 20 000°C, length less than 20 cm and width less than 10 cm and in this volume ~10 MW is released [2]. The heat transport from this extremely intense heat source is approximately equally distributed between radiation and convection [3], which easily heats the *inner reaction zone* to above 2 000°C. The reactions in the *outer reaction zone* get heat dissipated by the charge current, by the hot gases passing through the charge from the *inner reaction zone*, and by heat conduction due to the temperature gradients.

It is clear that there must be a balance between the power dissipated in the two reaction zones and therefore between the reaction rates in the two zones. If too much heat is produced in the burden and too little in the arc, the result will be a furnace filled with carbide and slag, producing mostly silica dust and little metal. If too much heat is released in the arc and too little in the charge, the furnace grows narrow and the high current load may overstress furnace equipment leading to increased maintenance need. Therefore it is of interest to evaluate the current distribution in the bowels of the furnace.

2   CURRENT DISTRIBUTION

The measurement campaign accounted for in this paper was done on a 48 MVA submerged arc ferrosilicon furnace at Elkem Icelandic Alloys plant in Grundartangi, southwest Iceland. Measurements of current and voltage waveforms were done in three periods: first under normal operation, then while the furnace was melted down for relining and finally during a start-up period while the furnace was run at reduced voltage following the relining of the furnace. The MFD (Magneto-Fluid-Dynamic) AC arc simulations for Si and FeSi furnaces, previously reported by the authors of this paper, have been compared to measurements, but comparison is somewhat complicated by the uncertainty involved in estimating the fraction of the phase current bypassing the arc through the charge. The main argument for doing measurements during the start-up period is that the electrode is slightly dipped into the coke bed and lifting the electrode just a few cm should ensure that no current bypasses the arc through direct contact with the bed. The main problem when comparing modelling results with measurements is the uncertainty in determining the gas composition in the arc region, which is open to infiltration of air. However, it was possible to evaluate the arc resistance as the current passes through zero for a pure arc. The current and voltage waveforms for the coke bed arc are then used in the treatment of similar measurements during normal operation.

3   DATA TREATMENT AND METHODOLOGY

The data collected were, in addition to the standard operating parameter database, current and voltage waveforms. The current measurements were done at the primary side of the transformers, while the voltage was measured between the electrode clamps and furnace bottom employing the so called Böckmann compensation to eliminate systematic errors. The sampling frequency during the melt down period was 2 kHz, or a resolution of 0.5 ms. This means that during the 20 ms period 40 measurement points were registered. In the start-up period on a coke bed a different sampling apparatus was used, with a 12.5 times higher resolution of 25 kHz, giving 500 measurement points each period.

The measured current is the *phase current, $i_{ph,i}$*, for each phase *i*. As the current passes from the electrode to the bowel of the furnace on its path to the other two electrodes, it is split into *arc current, $i_{arc,i}$*, and *charge current, $i_{ch,i}$*, that bypasses the arc through the charge. We then have the relationship:

$$i_{ph,i} = i_{arc,i} + i_{ch,i} \tag{4}$$

The measured Böckmann voltage or *phase voltage, $u_{ph,i}$* is composed of three components. The *arc voltage, $u_{a,i}$*, which is the voltage over the arc and charge in parallel, a *series resistance R_s*, which is the resistance both in the electrode and furnace below the arc. Finally there is the *induced voltage $u_{ind,i}$*, due to the self induction in the high-power furnace, or more specifically:

$$u_{ph,i} = u_{a,i} + u_{s,i} + u_{ind,i} = u_{p,i} + u_{ind,i} \tag{5}$$

$$u_{ind,i} = L_i * \frac{di_{ph,i}}{dt} \tag{6}$$

Here a lumped phase inductance L_i includes both the self inductance L_{ii} and mutual inductances M_{ij} according to:

$$L_i = L_{ii} - M_{ij} - M_{ki} + M_{jk} \tag{7}$$

The voltage induced in an AC furnace causes a phase shift in the voltage as compared with the current. That means the current and voltage do not pass zero at the same time and a so called Lissajous curve, showing $u_{ph,i}$ as a function of $i_{ph,i}$ has an oval shape as seen in Figures 1 and 2.

Approximate reactances are known for the furnace although the precise value for the *lumped inductance L_i* is not generally known, and is in fact variable, depending on conditions and current distribution in the furnace, it may be found by subtracting $L_i*di_{ph,i}/dt$ from the phase voltage $u_{ph,i}$ and optimizing L_i such that the resulting *power producing voltage, $u_{p,i}=u_{a,i}+u_{s,i}$* and $i_{ph,i}$ pass through zero simultaneously.

In an industrial furnace carrying currents of ~100 kA, the phase shift in the voltage is considerable and must be subtracted from the signal in order to get voltage waveforms that may be compared with simulations.

When $u_{ind,i}$ has been removed from the signal, the remaining $u_{p,i}$ represents the voltage over the arc and charge in parallel, in addition to the voltage fall over a series resistance R_s which may be assumed to be a pure "ohmic" resistance. In the pilot furnace measurements reported in INFACON11 [4] it was established that a mature hearth in a FeSi producing furnace is ohmic in nature, i.e. will not cause the formation of harmonics in the current or voltage waveform. That implies that the charge resistance $R_{ch,i}$ is constant over the 20 ms period, and that any variation in *lumped phase resistance* $r_{ph,i}$ within the period must be due to the arc, or more specifically to the time dependent arc resistance $r_{arc,i}$. The relation between the four resistances is:

$$r_{ph,i} = \frac{1}{1/r_{arc,i} + 1/R_{ch,i}} + R_{s,i}$$
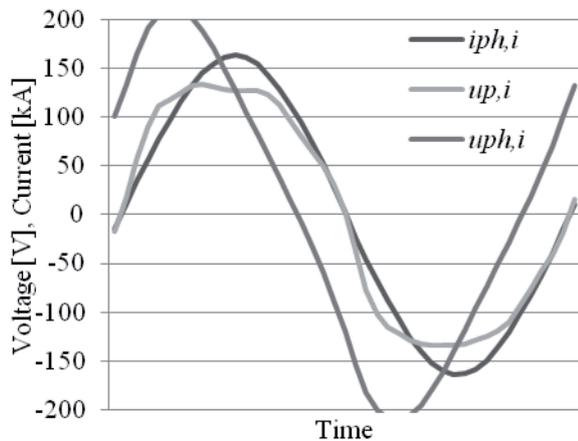
(8)

Figure 1: Typical measured current and voltage waveforms $i_{ph,i}$ and $u_{ph,i}$ along with the modified power producing voltage $u_{p,i}$ during normal furnace operation.
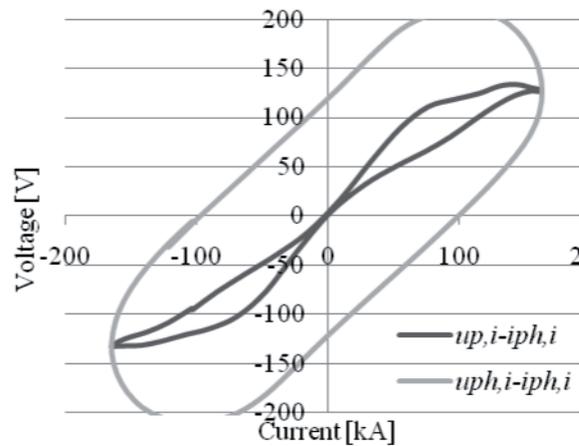

Figure 2: Typical Lissajous curves (corresponding to Figure 1) showing the measured $u_{ph,i}$ as well as $u_{p,i}$ as functions of $i_{ph,i}$.
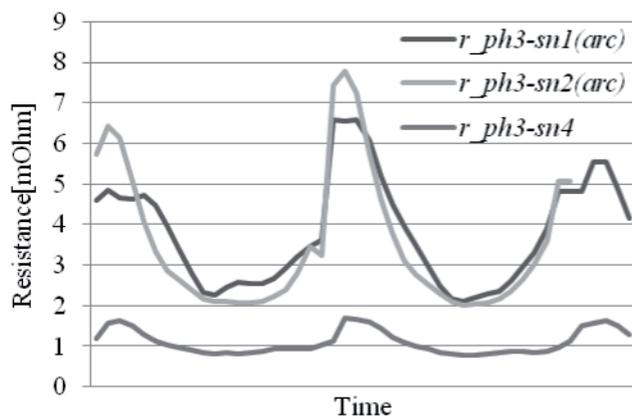

Figure 3: Resistance $r_{ph,3}$ as a function of time during an AC period. Sn1 and sn2 refer to a pure arc and sn4 to FeSi production operating conditions. The relevant values are given in Table 3. The spikes appear as the current passes zero.
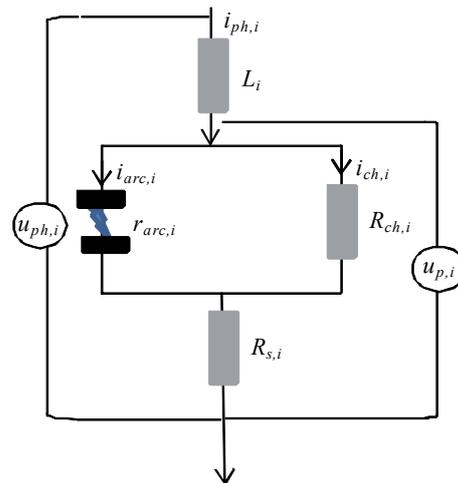

Figure 4: Schematic drawing of a configuration with a conducting charge resistance in parallel to the arc.

An AC electric arc will in general have a waveform that in each 10 ms half period may be divided into three intervals. The first is the interval as the phase current passes through current zero, and no heat is dissipated in the arc as would be needed to maintain the ionization level of the thermal plasma, of which the arc body is composed. In this interval the arc resistance is relatively high, considerably higher than in the part of the period when the current is near its maximum. As the current starts to flow and dissipate heat, the ionization level of the plasma increases with temperature and the resistivity decreases. Therefore the arc resistance reaches a minimum as the current has a maximum, and continues to be low during the third interval while the current is decreasing.

As the focus of this work is to estimate the fraction of the phase current that passes through the arc, the approach will be to look at the development of $r_{ph,i}$ over the period, and compare it to such development for a pure arc. Two separate waveform measurements were obtained for a pure arc in a 48 MVA industrial furnace at Icelandic Alloys discussed in section 4.1. Measured current and voltage waveforms obtained for *the pure arc* are shown in Figures 5 and 7, as well as those obtained from simulation as shown in Figures 14 and 15, are used to evaluate the time variability of the arc resistance $r_{arc,i}(t)$ within the 20 ms period. Those are in section 4.2 compared to simulations for an arc using the same furnace parameters as found in the furnace in question.

Finally the thus obtained arc resistance when passing through current zero, $R_{arc,0,i,}$ is used as an estimate to determine charge resistance for the furnace under normal FeSi75 producing operation, and thereby obtain a tentative estimate of the current distribution between arc and charge in section 4.3.

Phase resistance as a function of time is shown in Figure 3 for normal operation and pure arc operation. The zero crossing resistance $R_{ph,0,i,}$ may also be estimated by obtaining the slope of the Lissajous curve for $u_{p,i}$ and $i_{ph,i}$ at zero passage. The values shown in Tables 2 and 3 may be compared to the zero passage spike of the time dependent $r_{ph,3,}$ shown in Figure 3.

The "normal operation" waveforms for current $i_{ph,i}(t)$ and the power producing voltage $u_{p,i}(t)$, examples of which are shown in Figures 1, 20 and 22, seem indeed to be consistent with a pure arc burning in parallel to a charge resistance $R_{ch,i}$ which is linear, according to the lumped circuit model displayed in Figure 4.
In [1] it was found that the metallurgical charge in a metal producing furnace indeed appears to have a charge resistance that doesn´t produce harmonics: $R_{ch,i}$. Assuming that this is the case, that the charge resistance $R_{ch,i}$ is constant within the 20 ms period, then the electric arc must be the source of harmonics in the current and voltage waveforms. It will now be attempted to use this assumption to determine the fraction $i_{arc,i}(t)$ of the phase current $i_{ph,i}(t)$ that passes through the arc, and also the complimenting charge current $i_{ch,i}(t)$. Subsequently the power released in the arc and by ohmic heating of the charge can be determined.

The time variability of the lumped phase resistance $r_{ph,i}(t)$ within the 20 ms period is done by evaluating the instantaneous value of the resistance as it passes zero, $R_{ph,0,i}$, and compare to the effective phase resistance $R_{ph}=U_p/I_{ph}$. There are two conceivable ways to evaluate $R_{ph,0,i}$, using the measured $i_{ph,i}(t)$ and $u_{p,i}(t)$:
The direct way would be to plot $r_{ph,i}(t) = u_{p,i}(t) / i_{ph,i}(t)$, and read the resistance values directly. This approach is inconvenient due to two reasons: Insufficient sampling frequencies and slight inaccuracies in evaluating $u_{p,i}(t)$ from $u_{ph,i}(t)$ may lead to a large error in the resistance, because of slight time shift between current and voltage values when dividing by small numbers. Also zero point drift in the voltage measurement can lead to a large error in evaluating $r_{ph,i}(t)$ due to the same reason. A plot of $r_{ph,i}(t) = r_{arc,i}(t) + R_s$ for a pure arc as well as $r_{ph,i}(t)$ for a metal producing furnace is shown in Figure 3.
A less direct, but more accurate method is to plot the Lissajous curve for the $u_{p,i}(t)$ and $i_{ph,i}(t)$ signals. Such Lissajous curves for the pure arc are shown in Figures 6 and 8, and for the metal producing furnace in Figures 2, 19, 21 and 23. By evaluating the slope d $u_{p,i}$ /d $i_{ph,i}$ of the Lissajous curve as it passes zero, the zero passage resistance $R_{ph,0,i}$ is obtained**.** This method would be totally equivalent to using the peak values of the evaluated resistance $r_{ph,i}(t)$ obtained by method i), if there were no measurement errors involved. As this second approach in evaluating the resistance at zero crossing is more robust and not sensitive to zero point drift, it is used in the following analysis.

4   CURRENT AND VOLTAGE WAVEFORM MEASUREMENTS ON AN INDUSTRIAL FURNACE

Current and voltage waveforms were measured for the 48 MVA furnace at Icelandic Alloys during three different sets of operating conditions. First measurements were done while the furnace was operated at normal conditions for FeSi75 production. As the aim of the paper is to determine the distribution of the phase current between charge and arc, it is this first set of measurements that is analyzed with the aid of measured waveforms for a pure arc discussed in Section 4.1 and waveforms obtained by MHD simulations as discussed in Section 4.2. The measurements, data treatment and current distribution results for normal furnace operation are reported in Section 4.3.

4.1   Measured waveforms during pure arc operation

FeSi charge

As the furnace was prepared for relining, the furnace was run at decreasing load without charging. Consequently the raw material charge was smelted and discharged from the furnace, and measurements taken during that period of decreasing charge thickness until the electrode tip was exposed and pure arcing obtained. In this paper only snapshots for an isolated arc are shown from that period, as those are utilized in the subsequent analysis of data from normal operation. Snapshots for Figures 5, 6, 7 and 8 show current and voltage waveforms and Lissajous figures for two isolated arcs of different lengths. In a metal producing furnace under normal conditions the phase resistance variation within the 50 Hz period can be attributed to the electric arc. Therefore the resistance variation for the pure arc signal is used as a baseline. The *zero passage resistances* $R_{arc,0,i} + R_s$ obtained from the Lissajous curves using approach ii) proved to be $R_{arc,0,i} + R_s = 3.5$- 4.0 mΩ. and are listed in Table 2 along with other resistances.

Start-up on a coke bed

Following a relining of the furnace, measurements were performed on an industrial furnace during *start-up on a coke bed*. During the start-up period a coke bed surrounds the electrode tip, which is only immersed about ~10 cm deep in the bed. When the electrode is elevated there will probably be very little material in contact with the electrode, so it is plausible that the charge resistance $R_{ch,i}$ as defined in Figure 4 is very large and consequently the entire phase current goes through the arc. At the time of measurements**,** the load on the furnace was only about 15 MW. This gave the operators the freedom to indulge in the authors´ wishes for electrode manipulation.
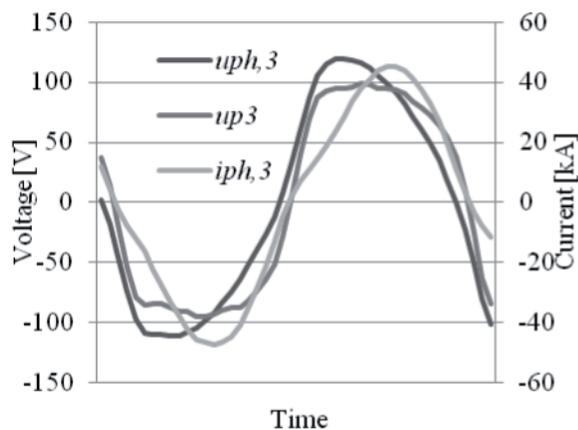

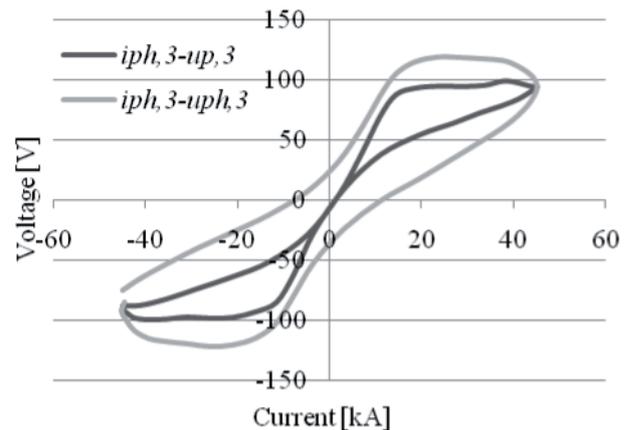**Figure 5:**   Waveforms for $i_{ph,3}$, $u_{ph,3}$ and $u_{p,3}$ as functions of time over a single 20 ms period.

Figure 6:   The zero passage resistance estimated from the Lissajous curve is $R_{arc,0,3} + R_{s,3} = 4$ mΩ.
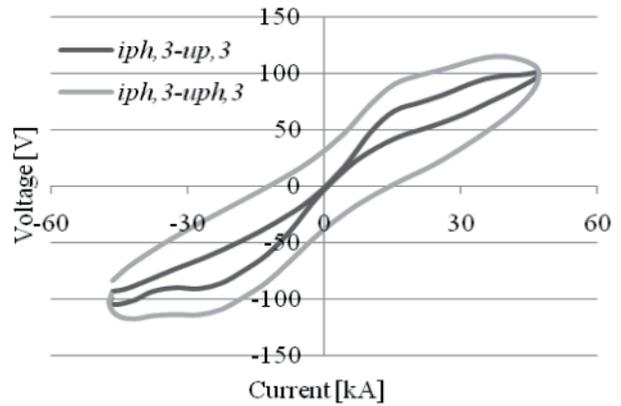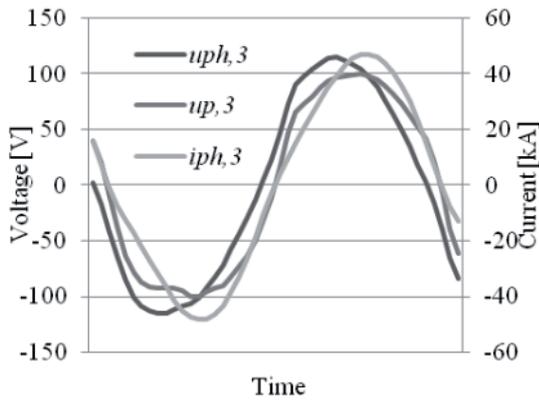
Figure 7: Waveforms for $i_{ph,3}$, $u_{ph,3}$ and $u_{p,3}$ as functions of time over a single 20 ms period.

Figure 8: The zero passage resistance estimated from the Lissajous curve is $R_{arc,0,3}+R_{s,3}$= 3.5 mΩ
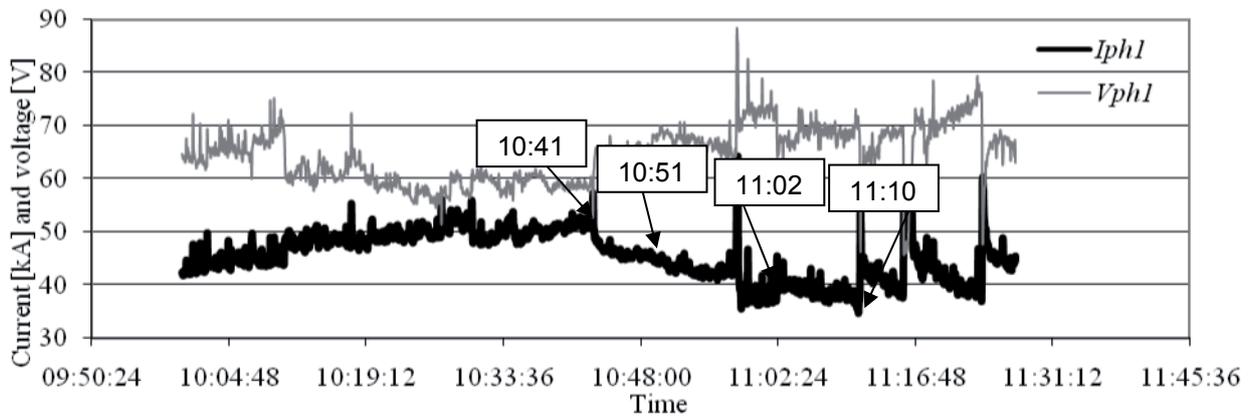

Figure 9: Start-up on a coke bed. Development of current and voltage over time for phase 1 in the furnace during furnace manipulation when electrode 1 was raised gradually above a coke bed. Marked on the figure are the instants of time for snapshots of the current and voltage waveforms
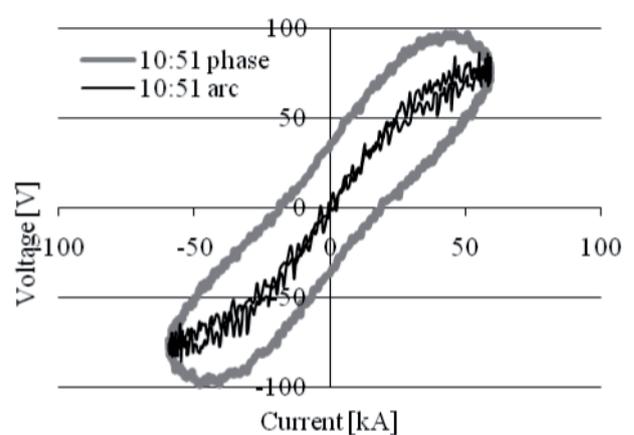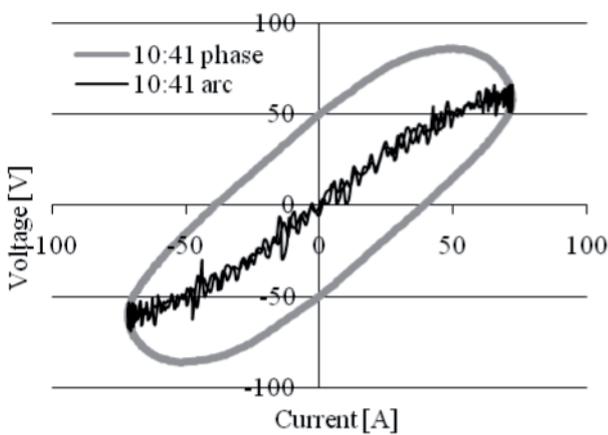

Figure 10: kA Lissajous figure from sn1 of electrode 1, insignificant (no?) arcing.
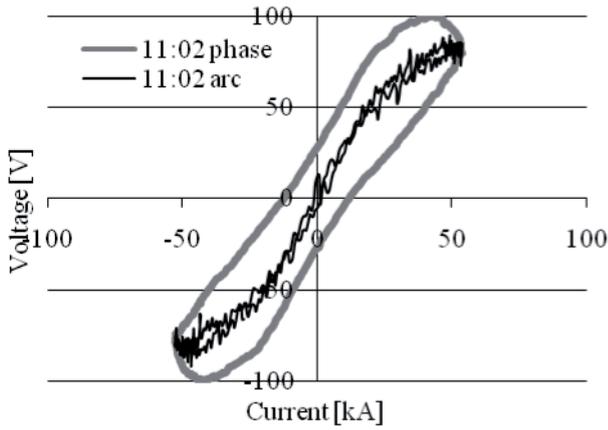
Figure 11: Lissajous figure of sn2
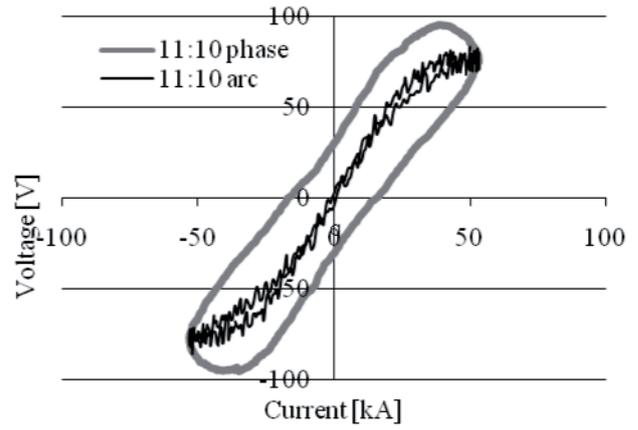
Figure 12: Lissajous figure of sn3

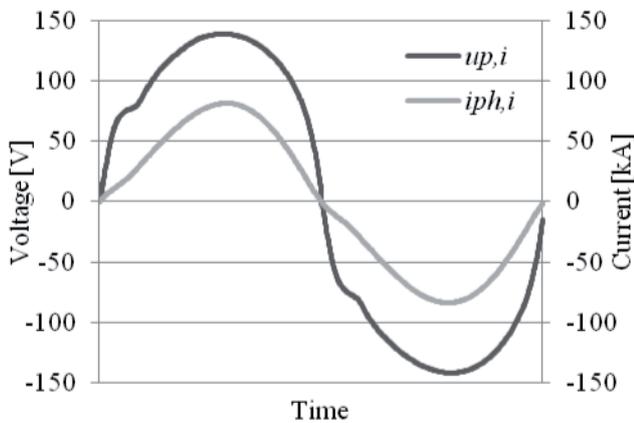**Figure 13:** Sn4, more significant arcing.

Figure 14: Simulated waveforms for $i_{ph,i}$ and $u_{p,i}$ for a 10 cm long arc shown as a function of time over a single 20 ms period.
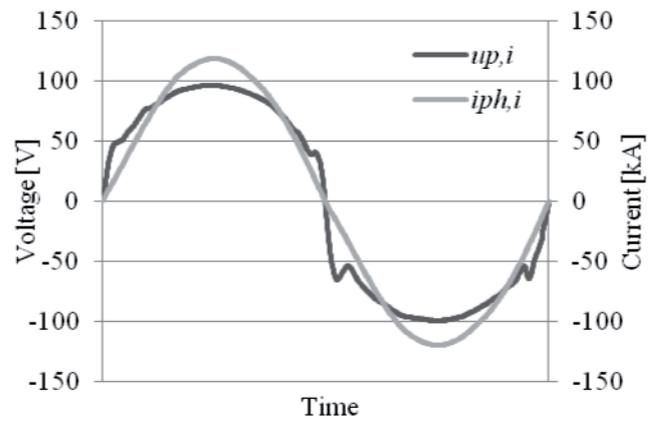

Figure 15: Simulated waveforms for $i_{ph,i}$ and $u_{p,i}$ for a 5 cm long arc shown as a function of time over a single 20 ms period
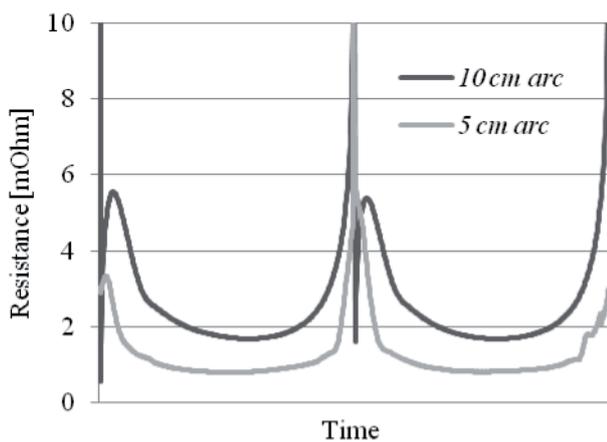

Figure 16: Time dependent arc resistance $r_{arc,i}(t) = u_{p,i}(t)/i_{ph,i}(t)$ for 10 and 5 cm long arcs burning in SiO:CO = 1:1 atmosphere, obtained by simulation.
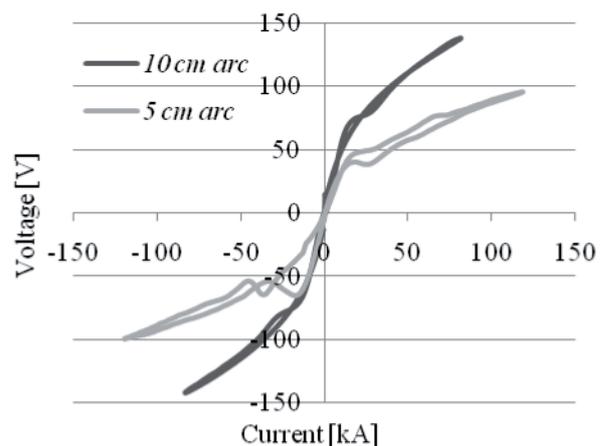

Figure 17: Lissajous figures for 10 and 5 cm long arcs burning in SiO:CO 1:1 atmosphere, obtained by simulation.

Table 1: Arc resistance at current zero derived from random snapshot measurements on an arc burning on a coke bed in a FeSi furnace.

$R_{ph0,i} + R_{s,i}$ [mΩ]– when passing zero			
	Phase 1	Phase 2	Phase 3
Snapshot 09:17	0.9	2.0	2.5
Snapshot 10:00	1.9	1.3	2.6
Snapshot 10:27	2.7	0.9	2.7
Snapshot 12:25	1.9	1.0	1.9
Snapshot 14:03	1.7	1.7	1.7
Snapshot 14:28	1.7	1.7	1.7

Figure 9 shows the RMS phase current and voltage development over a period when electrode 1 was gradually raised by 8 cm without changing the transformer settings. This caused a decrease in phase current from 50 kA to 34 kA. Four snapshots showing current and voltage waveforms are shown from this period, and the time at which the snapshots were taken is marked on Figure 9. In Figures 10, 11, 12 and 13, Lissajous curves for these snapshots are shown. The oval curve is the Lissajous curve for $u_{ph,i}$ as a function of $i_{ph,i}$, while the black curve in the centre is the modified power generating voltage $u_{p,i}$ as a function of current. The resistances obtained are also shown in Table 2. The general range in $R_{arc,0,i}$ is shown in Table 1 where estimates based on measurements done at random are displayed.

In general the figures show that when the electrode was raised, the phase resistance increased, the phase current decreased and the slope of the curves when passing through zero voltage increased. This slope of the Lissajous curve gives the phase resistance at zero current. Several current – voltage waveform snapshots were taken at random in an attempt to separate the voltage drop over the arc, and the voltage drop in the coke bed and furnace bottom. It was observed that the resistance when passing through zero varied between ~0.9 and 2.7 mΩ. When the resistance was at a minimum, the Lissajous figure was a straight line, exhibiting almost linear electric behaviour as shown for phase 2 in Figure 16. In those cases, the current probably was passing directly from the electrode through the coke bed without forming an electric arc. The non-linear coke bed behaviour observed in the pilot furnace was not found here, but there was some scrap iron present in the bed as well as iron from the electrode mantel. Linear behaviour was therefore expected. In other cases, the curvature and hysteresis of the Lissajous figure indicated the presence of an arc. From these estimates, given in Table 2, we assume that the resistance of the coke bed and furnace bottom is approximately 1mΩ, and the rest of the phase voltage drop is due to the arc.

Similar resistance measurements during furnace manipulation were obtained and are shown in Table 2 along with the result of a MFD arc simulation discussed in the next section. Before electrode 1 was elevated, the phase resistance was 1.2 mΩ, so there was relatively little arcing, which is supported by the relatively linear Lissajous diagram in Figure 10, with just a hint of arcing. This means that when the electrode had been elevated by 4 cm, the arc was probably not longer than 4 cm. By further elevation of the electrode the arc would move to the edge of the electrode and burn to a point on the wall of the hole in the coke bed, so probably the arc was only moderately longer when the electrode had been raised by 8 cm. Raising the electrode further almost extinguished the arc.

4.2 Numerical simulation of a pure arc

The authors of this paper have previously reported simulation models for AC electric arcs, where the MFD (Magneto- Fluid-Dynamic) equations are solved for the geometric and electric parameters of the furnace [4]. The simulations that are referred to in this paper, pertain to electric arcs in Si-metal or FeSi furnaces, where the plasma gas in the crater is composed of SiO and CO. The simulations were thus made using physical transport coefficients and radiation data for a 1:1 and 2:1 SiO-CO mixtures [4]. One of the results was that the calculated temperature field and current and voltage waveforms were not very sensitive to the SiO:CO ratio. Arcs have also been simulated with gas data including traces of Al and Ca [4,6,7,8]. The plasma composition above the coke bed is probably much richer in carbon species, and hardly includes any Si. As the normal chemical reactions involving the condensed phases $SiO_2(l)$, $Si(l)$ and $SiC(s)$ and the gaseous phase (SiO + CO) have not yet started, there must also be *nitrogen* species from infiltrated air present. In addition, iron species are probably also present in the arc region above the coke bed. Iron tends to increase the electric conductivity of

the arc plasma. However, as the required physical data for nitrogen and iron containing plasmas were not available, the simulation results should be interpreted bearing in mind that the arc plasma composition is different in the case of the coke bed.

For the open arc in the FeSi furnace, there are traces of Nitrogen in the arc atmosphere that are not included in the simulation, but otherwise the composition should be representative.

The simulated arcs presented here are implemented (placed) in a three phase furnace circuit model and the boundary conditions at the cathode are obtained from a Cathode/Anode sub-model presented in [7].

The slope of the Lissajous figures at zero passage for the simulated 5 cm and 10 cm SiO-CO arc, is compared to that of the measured curves in Table 3. It is seen that the simulated resistance ($R_{arc,0}$ + R_s) at zero current is 5 mΩ for the 10 cm long arc and 2.5 mΩ for the 5 cm long arc. These values are comparable to the resistance of the measured arc when the electrode has been raised by 6-8 cm above the coke bed. The arc extinguished shortly after this and the electrode was lowered in order to maintain the current. The measured FeSi arc ($R_{arc,0}$ + R_s) were in the range of ~3-4 mΩ, which fits well with the simulation results.

Table 2: Arc resistance at current zero derived from the snapshot measurements on an arc burning on a coke bed in a FeSi furnace and from MFD arc simulations of a 5 cm long arc in SiO-CO atmosphere.

	$R_{arc,0}$ +R_s [mΩ]
FeSi melt down: Snapshot Figures 7 and 8	4.0
FeSi melt down: Snapshot Figures 9 and 10	3.5
Coke bed: Snapshot 10:41	1.2
Coke bed: Snapshot 10:51	2.1
Coke bed: Snapshot 11:02	2.8
Coke bed: Snapshot 11:10	3.5
Simulation: 5 cm SiO-CO arc	2.5
Simulation : 10 cm SiO-CO arc	5.0

4.3 Current distribution at normal operation

Snapshots of waveforms of $i_{ph,i}$ and $u_{p,i}$ were examined at several random points in time with relatively symmetrical electrical conditions in the furnace. Symmetric conditions were sought as these would reduce the risk of errors in the measured phase voltage $u_{ph,i}$, due to a drift in the zero star-point in the furnace, but for sake of interest asymmetric cases are shown as well. Here the charge surrounds the electrode and carries current, as shown in the equivalent circuit in Figure 4. As demonstrated in Sections 4.1 and 4.2, *zero passage resistance $R_{arc,0}$ +R_s* for an isolated arc is between 2.5 and 4 mΩ.

In order to evaluate the percentage of phase current passing through the arc, the *zero passage phase resistance $R_{ph,0,i}$* was evaluated from *the slope* of the Lissajous figures. As the *charge resistance $R_{ch,i}$* is a constant in the timeframe of a 50 Hz period, upper and lower limits for $R_{ch,i}$ were obtained from Equation 5, assuming that $2.5 < R_{arc,0}$ +$R_s < 4$ mΩ. With this approach a maximum and minimum is obtained for the percentage of phase current passing through the arc, assuming that there is only one single arc burning in each phase. These values are shown in Table 3. It is probable that the arc in the crater has a $R_{arc,0}$ closer to the lower limit of ~2.5 mΩ, as there

is less cooling when it is burning in the crater. In addition no nitrogen is present in the crater, but for the open arc traces of nitrogen will lead to an increase in the low temperature resistivity due to the relatively high energy needed for splitting the molecule. Therefore the upper limit for the current is probably more reasonable at normal operating conditions.

The estimates in Table 3 assume that there is only one arc present in each phase, but if two arcs were present, for example in phase 1 of snapshot 6, that would lead to an estimated arc current fraction of 41%-64% instead of 23%-34%. It is therefore not unreasonable to imagine that unreasonably low $R_{ph,0,i}$ may be a sign of *multiple* arcs. Barker et. al.[9] have estimated a power fraction of 20-40% in the arc using a different approach, where they regard the arc and charge in series. That is however a similar power fraction as found here.

The results from the preceding analysis indicate that under normal operation approximately half of the current bypasses the arc through the charge. However, sometimes the waveforms indicate that either 2/3 of the current
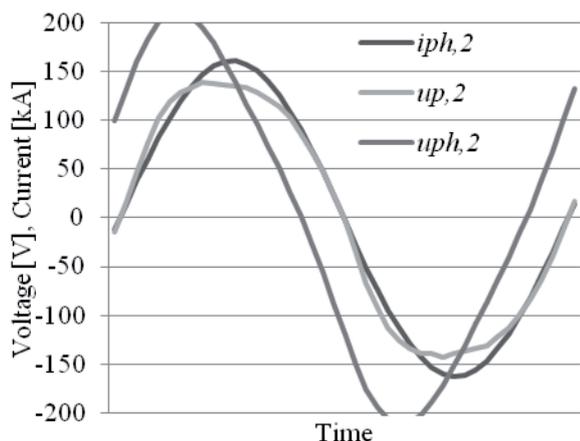
Figure 18: Waveforms of $i_{ph,2}$, $u_{ph,2}$ and $u_{p,2}$ are shown for snapshot sn1 (phase 2), as functions of time over a 20 ms period.
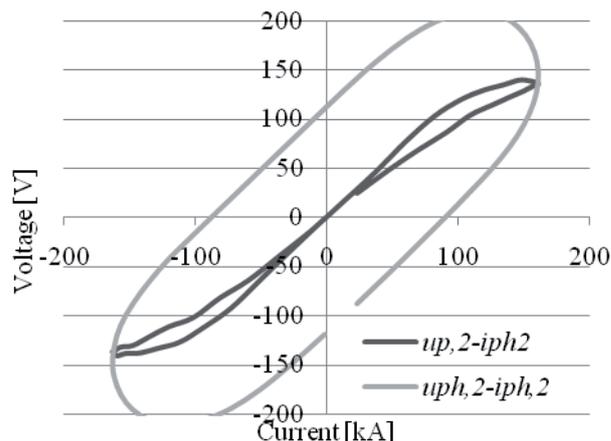
Figure 19: The zero passage resistance estimated from the Lissajous curve for snapshot sn1 is $R_{arc,0,3} + R_s$ = 1 mΩ, $0.38 < I_{arc,3}/I_{ph,3} < 0.52$
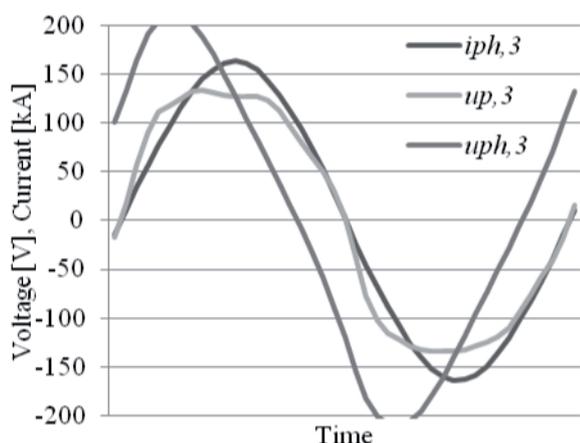

Figure 20: Waveforms of $i_{ph,2}$, $u_{ph,2}$ and $u_{p,2}$ are shown for snapshot sn2 (phase 3), as functions of time over a 20 ms period.

Figure 21: The zero passage resistance estimated from the Lissajous curve for snapshot sn2 is $R_{arc,0,3} + R_s$ = 1.27 mΩ, $0.51 < I_{arc,3}/I_{ph,3} < 0.$

Figure 22: Waveforms of $i_{ph,2}$, $u_{ph,2}$ and $u_{p,2}$ are shown for snapshot sn3 (phase 3), as functions of time over a 20 ms period.
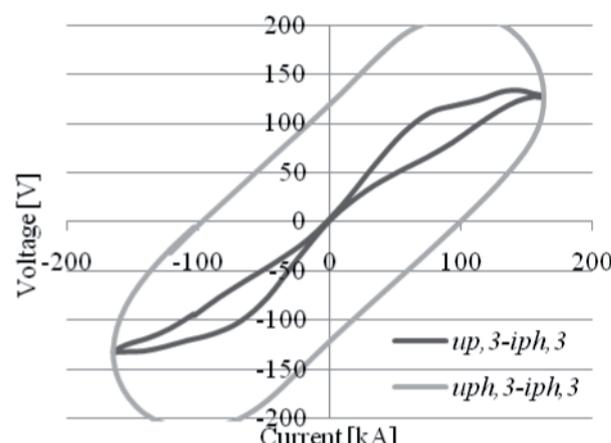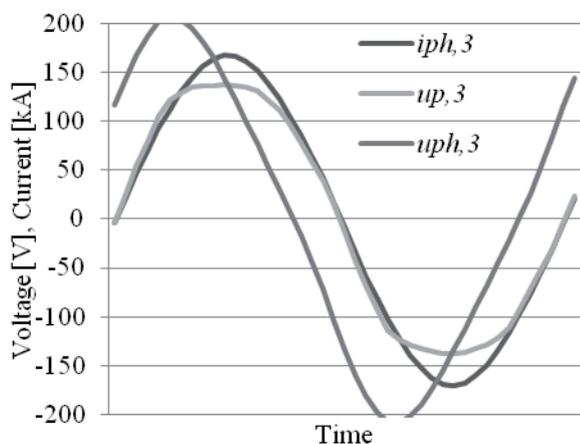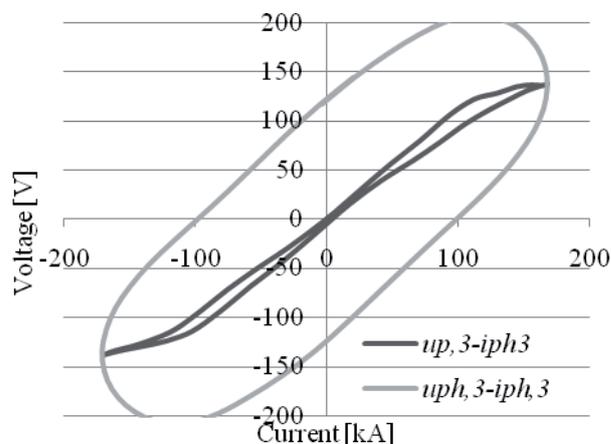
Figure 23: The zero passage resistance estimated from the Lissajous curve for snapshot n3 is $R_{arc,0,3} + R_s$ = 1.08 mΩ, $0.41 < I_{arc,3}/I_{ph,3} < 0.53$

Table 3: Zero passage phase resistance Rph,0,i, average phase resistance Rph,i, a maximum and minimum fraction of the phase current passing through the arc for all three phases at 6 different points in time, termed snapshots. The snapshots were done under normal furnace operation, and the current fraction estimates assume one arc per phase.

	Phase 1				Phase 2				Phase 3			
	$R_{ph,0}$ [mΩ]	$I_{arc,min}$	$I_{arc,max}$	R_{ph} [mΩ]	$R_{ph,0}$ [mΩ]	$I_{arc,min}$	$I_{arc,max}$	R_{ph} [mΩ]	$R_{ph,0}$ [mΩ]	$I_{arc,min}$	$I_{arc,max}$	R_{ph} [mΩ]
Snap-n1	1.15	47%	60%	0.87	1.00	38%	52%	0.82	1.30	51%	62%	0.97
Snap-n2	1.09	38%	46%	0.92	0.95	32%	45%	0.84	1.27	51%	65%	0.90
Snap-n3	1.00	30%	38%	0.92	0.91	28%	41%	0.84	1.08	40%	53%	0.88
Snap-n4	1.05	40%	52%	0.90	0.87	28%	41%	0.72	1.52	52%	69%	1.17
Snap-n5	1.09	40%	53%	0.90	1.01	38%	51%	0.84	1.00	37%	50%	0.83
Snap-n6	0.78	23%	34%	0.75	0.92	34%	46%	0.79	1.23	40%	56%	1.07

flows through the charge, or else that there are more than one arc present in that particular phase. The idea of *multiple arcs* is in fact not improbable as it would tend to be the physically most feasible situation for the system if the topology of the electrode and crater allows. Kaufmann´s minimum principle, which pertains to DC arcs, states that if the current-voltage characteristics of the arc is rising, i.e. dU_{arc}/dI_{arc} is positive, the voltage requirement of the arc is reduced by splitting the arc in two or more. That would be a more stable configuration, as the physical resistance is lowered. Simulations indicate that for the high-current AC arcs present in an industrial FeSi furnace, dU_{arc}/dI_{arc} is indeed positive and the characteristics rising [4,9]. If Kaufmann's principle is applicable to AC arcs, multiple arcs would therefore be likely if the geometry makes it feasible. Also multiple arcs is a more probable explanation for a large variability in the zero point phase resistance than a large variability in the charge resistance between three phases surrounded by a charge of the same composition.

5   CONCLUSIONS

The paper describes measurements of current and voltage waveforms done on an industrial Submerged Arc Furnace producing FeSi75. Measurements were done under normal operation, while the furnace was being emptied of charge before relining, and during start-up on a coke bed after relining. During the two latter periods current and voltage waveforms for an isolated arc were obtained, eliminating the effect of current bypassing the arc through the charge.

Current and voltage waveforms obtained from simulation by an advanced Magneto-Fluid-Dynamic electric arc model for this particular case, are shown and compared to the measured waveforms, showing acceptable accordance.

A method to evaluate the fraction of phase current passing through the charge is drafted and applied to the measurements shown in this paper, and indicates that under normal operation approximately 50% of the current bypasses the arc through the charge. The method is based on estimating the slope of the Lissajous curve at current zero, and is relatively robust to inaccuracies in phase voltage measurement. Sometimes the waveforms indicate that either 2/3 of the current is passing through the charge, or else that there are more than one arc present in that particular phase. As increasing the arc current tends to increase the arc voltage in the high-current industrial furnace, multiple arcs is probably a stable configuration.

6   REFERENCES

[1]   Schei A. Tuset J. Kr., Tveit H., "*Production of High Silicon Alloys*", TAPIR FORLAG, Trondheim 1998.

[2]   Saevarsdottir G.A., *"High Current AC Arcs in Silicon and Ferrosilicon Furnaces"*, Ph.D thesis, IME report 2002:36, Norwegian University of Science and Technology NTNU.

[3]   Eidem P.A., Tangstad M., and Bakken J.A., " Determination of Electrical Resistivity of Dry Coke Beds ", Metallurgical and Materials Transactions B, Volume 39, Number 1 / February, 2008

[4]   Saevarsdottir G. A., Magnusson T. and Bakken J. A., "Electric arc on a coke bed in a submerged arc furnace", In proceeding, Infacon 11, pp. 572-582

[5]   Sævarsdottir G.A., Bakken J.A., Sevastyanenko V.G., Gu Liping, "High-Power AC Arcs in Metallurgical Furnaces", J. High Temp. Material Processes, Sep. 2001, pp. 21-44.

[6]   Sævarsdottir G.A., Jonsson M.Th and Bakken J.A., "A novel approach to cathode/anode modelling for high current AC-arcs", ISPC-16, Taormina, June 2003. In Proceedings 3.7.

[7] Sævarsdottir G.A., Bakken J.A., Sevastyanenko V.G., Gu Liping, "Arc Simulation Model for Three-Phase Electro-Metallurgical Furnaces", INFACON 9, Quebec City, Canada, June 2001. Proceedings pp.253-263.

[8] Sævarsdottir G. A., Jonsson M.Th and Bakken J.A., "Arc-Electrode Interactions in Silicon and Ferrosilicon Furnaces", in Proceedings INFACON X, Cape Town, South Africa, Feb. 2004.

[9] Barker I.J., Rennie M.S., Hokadcay C.J. and Brereton-Stiles P.J., "Measurement and control of arcing in a submerged arc furnace", In proceedings, Infacon 11, pp. 685-694.

7   ACKNOWLEDGEMENTS